

1

September 1, 2020

2

The YR Polarimetry - Luminosity Monitor Chapter

3

4

5 Contents

6	0.1	Lepton and Hadron Polarimetry	1
7	0.1.1	Electron Polarimetry	3
8	0.1.2	Hadron Polarimetry	8
9	0.1.3	Luminosity Measurement:	11
10		References	R-1

11 0.1 Lepton and Hadron Polarimetry

12 Rapid, precise beam polarization measurements will be crucial for meeting the goals of
13 the EIC physics program as the uncertainty in the polarization propagates directly into the
14 uncertainty for relevant observables (asymmetries, etc.). In addition, polarimetry will play
15 an important role in facilitating the setup of the accelerator.

16 The basic requirements for beam polarimetry are:

- 17 • Non-destructive with minimal impact on the beam lifetime
- 18 • Systematic uncertainty on the order $\frac{dP}{P} = 1\%$ or better
- 19 • Capable of measuring the beam polarization for each bunch in the ring - in particular,
20 the statistical uncertainty of the measurement for a given bunch should be compara-
21 ble to the systematic uncertainty
- 22 • Rapid, quasi-online analysis in order to provide timely feedback for accelerator setup

23 0.1.1 Electron Polarimetry

24 The most commonly used technique for measuring electron beam polarization in rings
 25 and colliders is Compton polarimetry, in which the polarized electrons scatter from 100%
 26 circularly polarized laser photons. The asymmetry from this reaction is measured via the
 27 scattered electrons or high energy backscattered photons. A brief review and description
 28 of several previous Compton polarimeters can be found in [1]. A particular advantage of
 29 Compton polarimetry is that it sensitive to both longitudinal and transverse polarization.

30 The longitudinal analyzing power depends only on the backscattered photon energy and
 31 is given by,

$$A_{\text{long}} = \frac{2\pi r_0^2 a}{(d\sigma/d\rho)} (1 - \rho(1 + a)) \left[1 - \frac{1}{(1 - \rho(1 - a))^2} \right], \quad (1)$$

32 where r_0 is the classical electron radius, $a = (1 + 4\gamma E_{\text{laser}}/m_e)^{-1}$ (with the Lorentz factor
 33 $\gamma = E_e/m_e$), ρ is the backscattered photon energy divided by its kinematic maximum,
 34 $E_\gamma/E_\gamma^{\text{max}}$, and $d\sigma/d\rho$ is the unpolarized Compton cross section. In contrast, the transverse
 35 analyzing power depends both on the backscattered photon energy and the azimuthal
 36 angle (ϕ) of the photon (with respect to the transverse polarization direction);

$$A_{\text{tran}} = \frac{2\pi r_0^2 a}{(d\sigma/d\rho)} \cos \phi \left[\rho(1 - a) \frac{\sqrt{4a\rho(1 - \rho)}}{(1 - \rho(1 - a))} \right]. \quad (2)$$

37 This azimuthal dependence of the asymmetry results in an ‘‘up-down’’ asymmetry (as-
 38 suming vertically polarized electrons) and requires a detector with spatial sensitivity.

39 Plans for electron polarimetry at EIC include a Compton polarimeter at IP 12, where the
 40 electron beam is primarily vertically polarized. A Compton polarimeter near the primary
 41 detector in the vicinity of IP 6, where the beam will be a mix of longitudinal and transverse
 42 polarization, is also under investigation; since that region of the ring is extremely crowded,
 43 care must be taken in the assessment of whether a polarimeter can be accommodated. A
 44 schematic of the placement of the Compton polarimeter at IP 12 is shown in Fig. 1.

45 Nominal electron beam parameters at IP 12 are provided in Table 1. Of particular note is
 46 the relatively short bunch lifetime at 18 GeV. Table 2 shows the average transverse ana-
 47 lyzing power, luminosity, and time required to make a 1% (statistics) measurement of the
 48 beam polarization for an individual bunch, assuming a single Compton-scattered event
 49 per crossing. The constraint of having a single event per crossing is related to the need
 50 to make a position sensitive measurement at the photon and electron detectors. Note that
 51 even with this constraint, the measurement times are relatively short and, in particular,
 52 shorter than the bunch lifetime in the ring.

53 Even for a single electron bunch (circulating through the ring at a frequency of ≈ 75 kHz),
 54 the luminosities provided in Table 2 can be readily achieved using a single-pass, pulsed
 55 laser. Since the electron beam frequency varies with energy, it would be useful to have
 56 a laser with variable pulse frequency. A laser system based on the gain-switched diode
 57 lasers used in the injector at Jefferson Lab [2] would provide both the power and flexible

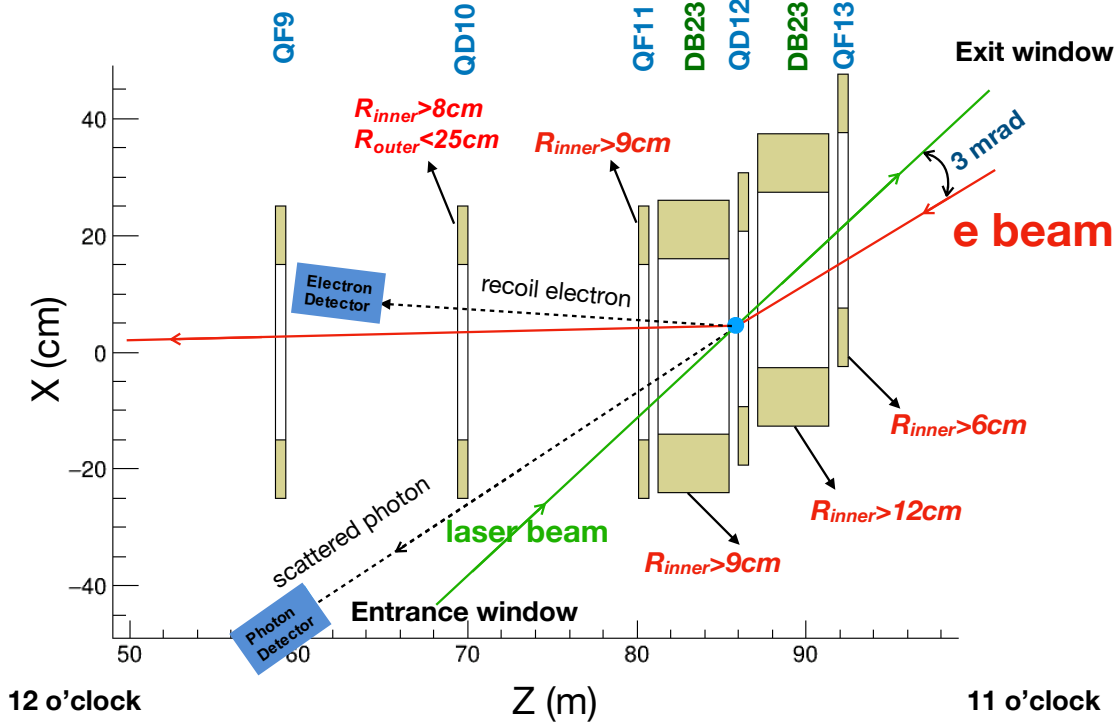


Figure 1: Layout of the Compton polarimeter at IP 12. In this figure the electron beam travels from right to left - the laser beam collides with the electrons just downstream of QD12. The dipole just downstream of the collision (DB12) steers the unscattered electrons allowing detection of the backscattered photons about 25 m downstream of the collision. DB12 also momentum-analyzes the scattered electrons, facilitating use of a position sensitive electron detector downstream of QD10. Also noted in the figure are constraints on required apertures of the magnets needed to allow transport of the laser beam, backscattered photons, and scattered electrons.

beam property	5 GeV	10 GeV	18 GeV
Bunch frequency	99 MHz	99 MHz	24.75 MHz
Beam size (x)	390 μm	470 μm	434 μm
Beam size (y)	390 μm	250 μm	332 μm
Pulse width (RMS)	63.3 ps	63.3 ps	30 ps
Intensity (avg.)	2.5 A	2.5 A	0.227 A
Bunch lifetime	>30 min	>30 min	6 min

Table 1: Beam parameters at IP12 for the EIC nominal electron beam energies.

58 pulse frequency desired. Such a system would make use of a gain-switched diode laser
 59 at 1064 nm, amplified to high average power (10-20 W) via a fiber amplifier, and then

beam energy [GeV]	σ_{unpol} [barn]	$\langle A_\gamma \rangle$	t_γ [s]	$\langle A_e \rangle$	t_e [s]	L[1/(barn·s)]
5	0.569	0.031	184	0.029	210	1.37E+05
10	0.503	0.051	68	0.050	72	1.55E+05
18	0.432	0.072	34	0.075	31	1.81E+05

Table 2: Asymmetries, measurement times needed for a 1% statistical measurement for one bunch and needed luminosities for three different beam energies for a 532 nm laser.

60 frequency doubled to 532 nm using a PPLN or LBO crystal. The repetition rate is set by
61 the applied RF frequency to the gain-switched seed laser.

62 The detector requirements for the EIC Compton polarimeters are dictated by the re-
63 quirement to be able to measure the transverse and longitudinal polarization simultane-
64 ously. For longitudinal polarization, this means the detectors will require sensitivity to the
65 backscattered photon and scattered electron energy. The photon detector can make use of
66 a fast calorimeter, while the electron detector can take advantage of the dispersion intro-
67 duced by the dipole after the collision point to infer the scattered electron energy from a
68 detector with position sensitivity in the horizontal direction.

69 To measure transverse polarization, position sensitive detectors are required to measure
70 the up-down asymmetry. This is particularly challenging given the very small backscat-
71 tered photon cone at the highest EIC beam energy. At HERA, the vertical position of the
72 backscattered photon was inferred via shower-sharing between the optically isolated seg-
73 ments of a calorimeter [3]. Calibration of the non-linear transformation between the true
74 vertical position and the energy-asymmetry in the calorimeter was a significant source of
75 uncertainty. The proposed detector for the EIC Compton will measure the vertical position
76 directly via segmented strip detectors, avoiding the calibration issues faced at HERA.

77 The transverse Compton analyzing power vs. position at the detector for the backscattered
78 photons and scattered electrons at 5 and 18 GeV is shown in Fig. 2. The backscattered pho-
79 ton cone will be largest at the lowest energy (5 GeV) - this will determine the required size
80 of the detector. The distribution at 18 GeV, where the cone is the smallest, sets the require-
81 ments for the detector segmentation. Note that the scattered electrons are significantly
82 more focused than the photons. Monte Carlo studies indicate that the transverse polariza-
83 tion can be reliably extracted at 18 GeV with a vertical detector segmentation of 100 μm
84 for the photon detector and 25 μm for the electron detector. The detector size should be at
85 least 16 x 16 mm² for the photons and 10 cm x 1 mm for the scattered electrons. The hor-
86 izontal segmentation for the electron detector can be much more coarse due to the large
87 horizontal dispersion introduced by the dipole.

88 Diamond strip detectors are a feasible solution for both the photon and electron detectors.
89 Diamond detectors are extremely radiation hard and are fast enough to have response
90 times sufficient to resolve the minimum bunch spacing (10 ns) at EIC. Tests of CVD di-
91 amond with specialized electronics have shown pulse widths on the order of 8 ns [4].
92 For the photon detector, about 1 radiation length of lead will be placed in front of the
93 strip detectors to convert the backscattered photons. As an alternative to diamond detec-

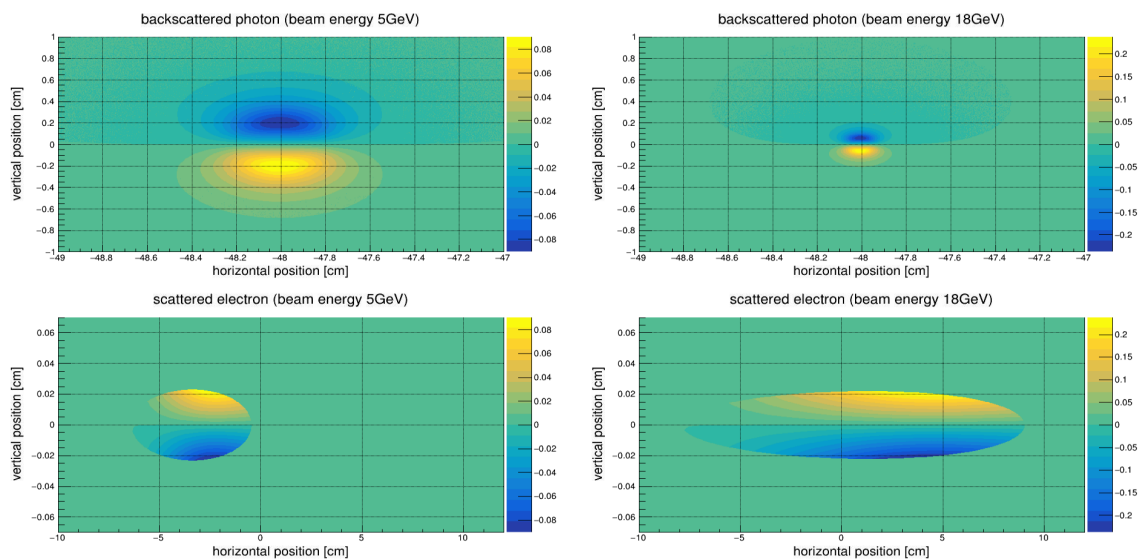


Figure 2: Compton (transverse) analyzing power at the nominal photon and electron detector positions for the IP 12 polarimeter.

94 tors, HVMAPS detectors are also under consideration. The radiation hardness and time
 95 response of HVMAPS will need to be assessed to determine their suitability for this appli-
 96 cation.

97 As noted earlier, the photon detector will also require a calorimeter to be sensitive to longi-
 98 tudinal components of the electron polarization. Only modest energy resolution is needed;
 99 radiation hardness and time response are more important requirements for this detector -
 100 a tungsten powder/scintillating fiber calorimeter would meet these requirements.

101 Backgrounds are an important consideration for Compton polarimetry as well. The pri-
 102 mary processes of interest are Bremsstrahlung and synchrotron radiation. Monte Carlo
 103 studies have shown that the contribution from Bremsstrahlung should be small for a beam-
 104 line vacuum of 10^{-9} Torr. Synchrotron radiation, on the other hand, will be a significant
 105 concern. Careful design of the exit window for the backscattered photons will be required
 106 to mitigate backgrounds due to synchrotron. The electron detector is not in the direct syn-
 107 chrotron fan, but significant power can be deposited in the detector from one-bounce pho-
 108 tons. This can be mitigated by incorporating tips or a special antechamber in the beampipe
 109 between the Compton IP and the detector [5]. The electron detector will also be subject to
 110 power deposited in the planned Roman Pot housing due to the beam Wakefield. Pre-
 111 liminary simulations indicate the Wakefield power should not be large enough to cause
 112 problems, but this will need to be considered in the detailed Roman Pot design.

113 In addition to measurements in the EIC electron ring, it is important to be able to deter-
 114 mine the electron beam polarization in or just after the Rapid Cycling Synchrotron (RCS) in
 115 order to facilitate machine setup and troubleshoot possible issues with the electron beam
 116 polarization. In the RCS, electron bunches of approximately 10 nC are accelerated from
 117 400 MeV to the nominal beam energy (5, 10, or 18 GeV) in about 100 ms. These bunches

118 are then injected into the EIC electron ring at 1 Hz. The short amount of time each bunch
 119 spends in the RCS, combined with the large changes in energy (and hence polarimeter
 120 analyzing power and/or acceptance) make non-invasive polarization measurements, in
 121 which the the RCS operates in a mode completely transparent to beam operations, essen-
 122 tially impossible. However, there are at least two options for making intermittent, invasive
 123 polarization measurements.

124 The first, and perhaps simplest from a polarimetry perspective, would be to operate the
 125 RCS in a so-called “flat-top” mode [6]. In this case, an electron bunch in the RCS is accel-
 126 erated to its full or some intermediate energy, and then stored in the RCS at that energy
 127 while a polarization measurement is made. In this scenario, a Compton polarimeter sim-
 128 ilar to that described above could be installed in one of the straight sections of the RCS.
 129 The measurement times would be equivalent to those noted in Table 2 (since those are for
 130 a single stored bunch), i.e., on the order of a few minutes.

131 Another option would be to make polarization measurements in the transfer line from the
 132 RCS to the EIC electron ring. In this case, one could only make polarization measurements
 133 averaged over several bunches. In addition, the measurement would be much more time
 134 consuming due to the low average beam current (≈ 10 nA) since the 10 nC bunches are
 135 extracted at 1 Hz.

136 The measurement time at 10 nA using a Compton polarimeter similar to the one planned
 137 for IP12 would take on the order many days. The IP12 Compton limits the number of inter-
 138 actions to an average of one per crossing to be able to count and resolve the position of the
 139 backscattered photons. A position sensitive detector that could be operated in integrating
 140 mode, would allow more rapid measurements. However, the required position resolution
 141 (25-100 μm) would be very challenging for a detector operating in integrating mode.

142 An alternative to Compton polarimetry would be the use of Møller polarimetry. Møller
 143 polarimeters can be used to measure both longitudinal and transverse polarization and can
 144 make measurements quickly at relatively low currents. The longitudinal and transverse
 145 Møller analyzing powers are given by,

$$A_{ZZ} = -\frac{\sin^2 \theta^* (7 + \cos^2 \theta^*)}{(3 + \cos^2 \theta^*)^2}, \quad (3)$$

$$A_{XX} = -\frac{\sin^4 \theta^*}{(3 + \cos^2 \theta^*)^2}, \quad (4)$$

146 where A_{ZZ} is the analyzing power for longitudinally polarized beam and target electrons,
 147 A_{XX} for horizontally polarized beam and target electrons, and θ^* is the center-of-mass
 148 scattering angle. Note that $A_{YY} = -A_{XX}$. The magnitude of the analyzing power is maxi-
 149 mized in both cases at $\theta^* = 90$ degrees, where $|A_{ZZ}| = 7/9$ and $|A_{XX}| = 1/9$.

150 Extrapolating from typical measurement times from the Møller polarimeters at Jefferson
 151 Lab (which provide a statistical precision of 1% for the longitudinal polarization in about
 152 15 minutes for a 1 μA beam on a 4 μm iron target), we estimate that a 10% measurement
 153 could be made in about 1.5 hours in the RCS to EIC transfer line. This could perhaps

154 be shorter depending the maximum foil thickness that could be used as the polarimeter
155 target.

156 A key drawback of Møller polarimetry is that the solid foil targets are destructive to the
157 beam, so cannot be carried out at the same time as normal beam operations. An additional
158 complication is the requirement for a magneto-optical system to steer the Møller electrons
159 to a detector system. In the experimental Hall A at Jefferson Lab, the Møller spectrometer
160 employs several quadrupoles of modest length and aperture, combined with a dipole to
161 deflect the Møller electrons into the detector system. The whole system occupies about
162 7 m of space along the beamline, but the space used by the quadrupoles can also be used
163 for beam transport during normal operations (i.e., when Møller measurements are not
164 underway).

165 The preferred choice for polarimetry at the RCS is a Compton polarimeter in the RCS ring,
166 with measurements taking place during “flat-top” mode operation. However, if this “flat-
167 top” mode is not practical, then a Møller polarimeter in the RCS transfer line could serve
168 as a reasonable fallback, albeit with reduced precision and a larger impact on the beamline
169 design.

170 0.1.2 Hadron Polarimetry

171 Hadron polarimetry has been successfully performed on RHIC polarized proton beams for
172 nearly two decades. Through continual development a systematic uncertainty $\sigma_p^{\text{sys}}/P <$
173 1.5% [7] was achieved for the most recent RHIC polarized proton run. After improving
174 data analysis, systematic uncertainties in measurement of the beam profile averaged po-
175 larization were reduced to $\sigma_p^{\text{sys}}/P \lesssim 0.5\%$ [8]. As the only hadron polarimeter system at a
176 high energy collider it is the natural starting point for hadron polarimetry at the EIC.

177 Hadron polarization is typically measured via a transverse single spin left right asymme-
178 try: $\epsilon = A_N P$. Unlike for polarized leptons, the proportionality constant is not precisely
179 known from theory. The solution at RHIC employs an absolute polarimeter with a polar-
180 ized atomic hydrogen jet target (HJET) [9], illustrated in Fig. 3. The hydrogen polarization
181 vector is alternated between vertically up and down. The RHIC beam also has bunches
182 with up and down polarization states. By averaging over the beam states the asymmetry
183 with respect to the target polarization may be measured, and vice versa:

$$\epsilon_{\text{target}} = A_N P_{\text{target}} \quad \epsilon_{\text{beam}} = A_N P_{\text{beam}} . \quad (5)$$

184 The target polarization is precisely measured with a Breit-Rabi polarimeter. Combined
185 with the measured asymmetries the beam polarization is determined:

$$P_{\text{beam}} = \frac{\epsilon_{\text{beam}}}{\epsilon_{\text{target}}} P_{\text{target}} . \quad (6)$$

186 The absolute polarization measurement is independent of the details of A_N .

187 Even though, the diffuse nature of the polarized jet target provides only a relatively low

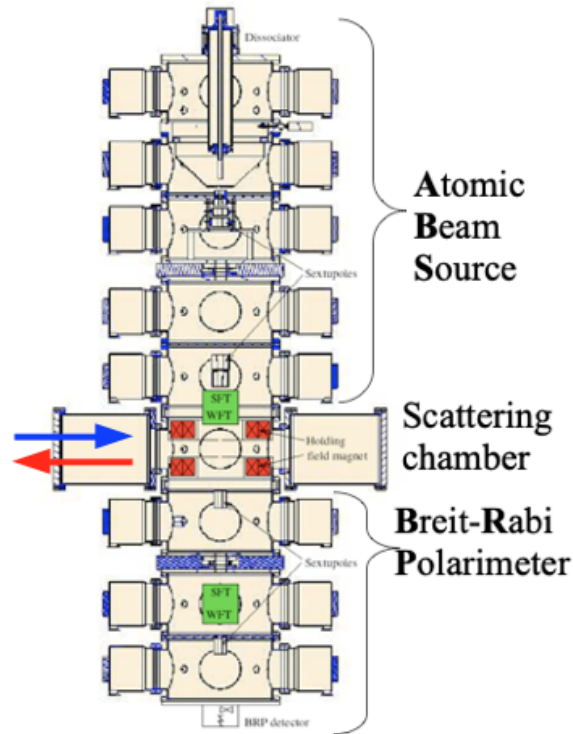


Figure 3: The RHIC polarized hydrogen jet polarimeter. The atomic beam source at the top passes polarized hydrogen across the beams (blue and red arrows) in the scattering chamber, with detectors left and right of the beams. The atomic hydrogen polarization is measured by the Breit-Rabi polarimeter at bottom.

188 rate of interactions, continuous operation during the store resulted in statistical precision
 189 of the polarization measurement of about $\sigma_p^{\text{stat}} \sim 2\%$ per 8-hour RHIC fill (in Run 17).
 190 These measurements, however, are not sensitive to the inevitable decay of beam polariza-
 191 tion throughout a fill. Also, the jet target is wider than the beam and measures only the
 192 average polarization across the beam. The beam polarization is larger at the center than
 193 the edges transversely; the polarization of colliding beams differs from the average polar-
 194 ization due to this effect [10]. The polarimeters must measure this transverse polariza-
 195 tion profile to provide correct polarizations for use by collider experiments.

196 At RHIC the required finer grained polarization details are provided by the proton-carbon
 197 (pC) relative polarimeter, illustrated in Fig. 4. A thin carbon ribbon target is passed
 198 across the beam and scattered carbon nuclei are measured in detectors arrayed around the
 199 beam. The dense target provides a high interaction rate, allowing an asymmetry measure-
 200 ment with a few per cent statistical precision in less than 30 seconds. Such measurements
 201 are made periodically throughout a RHIC fill, providing a measurement of the beam polariza-
 202 tion decay. The ribbon target is narrower than the beam; thus it is able to measure asym-
 203 metry as a function of position across the beam and determine the transverse polariza-
 204 tion profile. The absolute polarization scale of the pC polarimeter is set by normalizing an en-
 205 semble of pC measurements to the results from the Hjet polarimeter for the corresponding

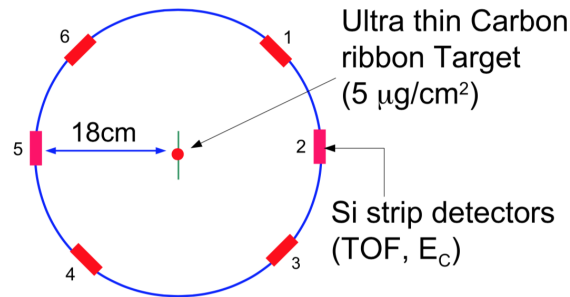


Figure 4: Cross section of the RHIC proton-carbon polarimeter. A thin carbon ribbon target is passed across the beam (into page) and scattered carbon nuclei are measured in the six detectors.

207 Both of the RHIC hadron polarimeters can in principle be used for proton polarimetry at
 208 the EIC. At present two significant difficulties are foreseen. First, backgrounds in both po-
 209 larimeters are observed and lie partially beneath the signal events. They are distinguished
 210 by timing distributions different from the signal allowing separation or estimation of a
 211 subtraction from the signal. At the EIC with higher bunch crossing frequency, the back-
 212 grounds will lie under the signal events from adjacent bunches and separation or subtrac-
 213 tion based on timing will not be possible. Studies are under way to determine the nature
 214 of the background and possibly find a rejection method. Second, materials analysis of the
 215 carbon ribbon targets indicates that the the higher proton beam currents and bunch cross-
 216 ing frequencies at the EIC will induce heating to temperatures causing the targets to break
 217 after only a few seconds in the beam. A search for alternative target materials has been
 218 initiated.

219 A possible alternative to the pC polarimeter has been proposed. It is based on the obser-
 220 vation by the PHENIX collaboration of a large azimuthal asymmetry of forward neutrons
 221 in the proton direction in $p+Au$ collisions [11]. This effect is well described by a process
 222 of the high Z Au nucleus emitting a photon, which produces neutrons off of the polarized
 223 proton [12]. A polarimeter based on this process would replace the Au beam with a high Z
 224 fixed target as a source of photons; a Xe gas jet may be a suitable target. Such a polarimeter
 225 could be tested at RHIC in the final years of operation.

226 For light ion polarimetry at the EIC, the following methods can be considered:

- 227 – Using a polarized light ion jet target. Similarly to the proton beam measurement with
 228 hydrogen jet target, the light ion beam polarization is given by Eq. (6). Tagging of breakup
 229 of beam nuclei may be necessary to isolate the elastic scattering signal required for an abso-
 230 lute polarization measurement. However, a preliminary evaluation, based on deuterium
 231 beam scattering at HJET, indicates that the breakup contamination of the elastic data is
 232 small, only few percent, and, thus, the correction to Eq. (6) is expected to be negligible.
- 233 – Using polarized hydrogen jet target to measure light ion, e.g. He-3 (h), beam polar-
 234 ization. Since the beam and target particles are not identical, Eq. (6) should be corrected

$$P_{\text{beam}} = \frac{\epsilon_{\text{beam}}}{\epsilon_{\text{target}}} P_{\text{target}} \times \frac{\kappa_p - 2\text{Im} r_5^p - 2\text{Re} r_5^p T_R/T_c}{\kappa_h - 2\text{Im} r_5^h - 2\text{Re} r_5^h T_R/T_c} \quad (7)$$

236 where, $\kappa_p = \mu_p - 1 = 1.793$ and $\kappa_h = \mu_h/2 - 1/3 = -1.398$ are parameters derived
 237 from magnetic moments of proton and He-3, r_5^p and r_5^h are hadronic spin flip ampli-
 238 tudes [13] for hp^\uparrow and $h^\uparrow p$ scattering, respectively, T_R is the recoil proton kinetic energy
 239 and $T_c = 4\pi\alpha Z_h/m_p\sigma_{\text{tot}}^{hp} \approx 0.7\text{ MeV}$. Since $|r_5| = \mathcal{O}(1\%)$ are small, such measured ab-
 240 solute He-3 beam polarization will meet the EIC requirement if r_5^p and r_5^h can be related,
 241 with theoretical uncertainties better than 30–50%, to the proton-proton r_5 experimentally
 242 determined at HJET [14].

243 – Using low energy technique, e.g. [15], determine absolute light ion polarization in
 244 source and, then, monitor beam polarization decay and profile with beam acceleration
 245 control tools. This method is expected to work well if the beam polarization losses will be
 246 small at EIC. However, for a precision calibration, alternative measurements of the abso-
 247 lute polarization may be needed.

248 The pC polarimeter or an alternative developed for protons at the EIC should also provide
 249 suitable relative polarimetry for light ions.

250 The main polarimeters may be situated anywhere in the EIC hadron ring. The Hjet and
 251 pC polarimeters each require 1-2 m space along and transverse to the beam. However, one
 252 relative polarimeter (pC or alternative) should be placed near the experimental interaction
 253 point between the hadron spin rotators. The hadron polarimeters are only sensitive to
 254 transverse spin polarization. During longitudinal spin runs asymmetry measurements
 255 near the interaction point are required to verify that the transverse component of the spin
 256 direction is zero.

257 0.1.3 Luminosity Measurement:

258 The luminosity measurement provides the required normalization for all physics studies.
 259 At the broadest scale it determines absolute cross sections, such as needed for the structure
 260 function F_2 and derived PDFs. On an intermediate scale, it is also required to combine dif-
 261 ferent running periods, such as runs with different beam energies needed to measure F_L ,
 262 or runs with different beam species to study A dependencies. Asymmetry measurements
 263 are conducted using beams with bunches of both spin states. On the finest scale, the rela-
 264 tive luminosity of the different bunch crossings is needed to normalize the event rates for
 265 the different states; the uncertainty on the relative bunch luminosity is a limiting factor for
 266 asymmetry measurements.

267 The bremsstrahlung process $e + p \longrightarrow e + p + \gamma$ was used successfully for the measure-
 268 ment of luminosity by the HERA collider experiments [16–18]. It has a precisely known
 269 QED cross-section which is large, minimizing theoretical uncertainty and providing negli-
 270 gible statistical uncertainty. Thus the scale uncertainty of the luminosity is determined by
 271 the systematic uncertainties of the counting of bremsstrahlung events. The ZEUS collabo-
 272 ration at HERA measured luminosity with a 1.7% scale uncertainty; further improvements

273 at the EIC should be able to reduce this to $<1\%$ as required by the physics program.

274 In contrast to HERA, where only the electron beam was polarized, both the electron and
 275 proton/light ion beams will be polarized in the EIC. In this case the bremsstrahlung rate
 276 is sensitive to the polarization dependent term $a(P_e, P_h)$ in the cross section $\sigma_{\text{brems}} =$
 277 $\sigma_0(1 + a(P_e, P_h))$. Thus, the polarizations P_e, P_h and luminosity measurements are coupled,
 278 and the precision of the luminosity measurement is limited by the precision of the polar-
 279 ization measurement. This is especially important for relative luminosities for asymmetry
 280 measurements, where the bremsstrahlung process used for normalization has different
 281 cross sections for different spin states. The precision needed for the relative luminosity
 282 measurement is driven by the magnitude of the physics asymmetries which can be as low
 283 as 10^{-4} ; the uncertainty on relative bunch luminosities must reach this level of precision.

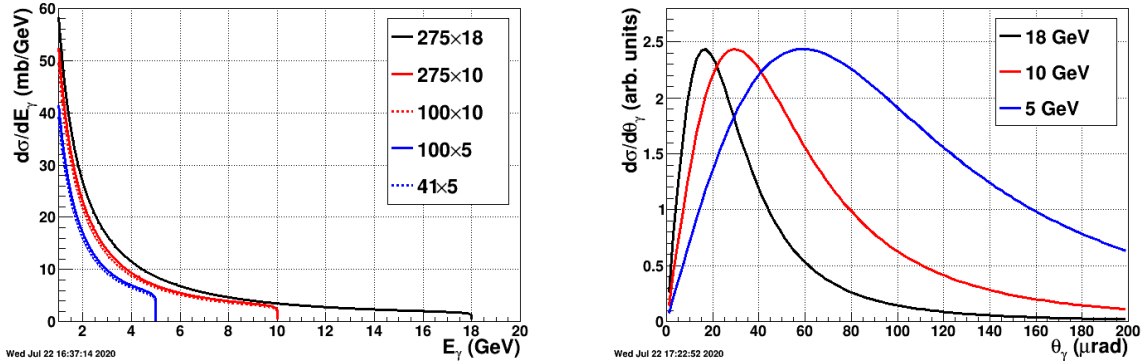


Figure 5: Bremsstrahlung photon energy (left) and angular (right) distributions for EIC beam energies.

284 The bremsstrahlung photon energy E_γ distributions for EIC beam energies are shown in
 285 the left of Fig. 5. They diverge as $E_e \rightarrow 0$ and have sharp cutoffs at the electron beam
 286 energies. As shown in the right of Fig. 5, the bremsstrahlung photons are strongly peaked
 287 in the forward direction with typical values of $\theta_\gamma \approx m_e/E_e$, with values of 20-60 μrad at
 288 the EIC. The RMS angular divergence of the electron beam is significantly larger than these
 289 values and will dominate the angular distribution of bremsstrahlung photons.

290 **Bremsstrahlung Photon Detectors:** The straightforward method for measuring
 291 bremsstrahlung situates a calorimeter at zero degrees in the electron direction counting
 292 the resulting photons, as shown lower left of Fig. ???. The calorimeter is also exposed to
 293 the direct synchrotron radiation fan and must be shielded, thus degrading the energy
 294 resolution. This also imposes a rough low energy cutoff on photons typically ≈ 0.1 -1 GeV
 295 below which the calorimeter is insensitive. At peak HERA luminosities, the photon
 296 calorimeters were sensitive to 1-2 photons per HERA bunch crossing. At an EIC luminos-
 297 ity of $10^{33} \text{ cm}^{-2} \text{ s}^{-1}$, the mean number of such photons per bunch crossing is over 20 for
 298 electron-proton scattering and increases with Z^2 of the target for nuclear beams. The per
 299 bunch energy distributions are broad, with a mean proportional to the number of photons

300 per bunch crossing. The counting of bremsstrahlung photons thus is effectively an energy
301 measurement in the photon calorimeter with all of the related systematic uncertainties
302 (e.g. gain stability) of such a measurement.

303 An alternative method to counting bremsstrahlung photons, used effectively by the ZEUS
304 collaboration at HERA, employs a pair spectrometer. A small fraction of photons is con-
305 verted into e^+e^- pairs in the vacuum chamber exit window. A dipole magnet splits the
306 pairs vertically and each particle hits a separate calorimeter adjacent to the unconverted
307 photon path. The relevant components are depicted in the lower left of Fig. ???. This has
308 several advantages over a zero-degree photon calorimeter:

- 309 • The calorimeters are outside of the primary synchrotron radiation fan.
- 310 • The exit window conversion fraction reduces the overall rate.
- 311 • The spectrometer geometry imposes a low energy cutoff in the photon spectrum,
312 which depends on the magnitude of the dipole field and the location of the calorime-
313 ters.

314 The variable parameters of the last two points (conversion fraction, dipole field and
315 calorimeter locations) may be chosen to reduce the rate to less than or of order one e^+e^-
316 coincidence per bunch crossing even at nominal EIC luminosities. Thus, counting of
317 bremsstrahlung photons is simply counting of e^+e^- coincidences in a pair spectrometer
318 with only small corrections for pileup effects.

319 The locations of a zero-degree calorimeter and pair spectrometer are shown in the bottom
320 left of Fig. ???. Careful integration into the machine lattice is required, not only to allow
321 for enough space for the detectors, but also to accommodate the angular distribution of
322 the photons. This is dominated by the angular divergence of the electron beam, with RMS
323 values as high 0.2 mrad. Thus a clear aperture up to a few mrad is required to measure
324 the angular distribution and minimize the acceptance correction. The spectrometer rate
325 is directly proportional to the fraction of photons which convert into e^+e^- pairs, plac-
326 ing stringent requirements on the photon exit window. It must have a precisely known
327 material composition, and a precisely measured and uniform thickness along the photon
328 direction.

329 Calorimeters are required for both luminosity devices, for triggering and energy mea-
330 surements. The high rates dictate a radiation hard design, especially for the zero-degree
331 calorimeter, which must also have shielding against synchrotron radiation. The spectrom-
332 eter must also have precise position detectors to measure the e^\pm . Combined with the
333 calorimeter energy measurement this allows reconstruction of the converted photon po-
334 sitions. The distribution of photon positions is required to correct for the lost photons
335 falling outside the photon aperture and detector acceptances.

336 **Bremsstrahlung and Low- Q^2 Electron Detectors:** Downstream of the interaction point
337 the electron beam is accompanied by a flux of electrons at small angles with respect to the

338 beam direction and at slightly lower energy. They are predominantly final state electrons
 339 from the bremsstrahlung process $e + p \rightarrow e + p + \gamma$, with an energy distribution the
 340 mirror image of the left of Fig. 5 with $E'_e = E_e - E_\gamma$. Also, a fraction of the electrons in this
 341 region are produced in quasi-real photoproduction with $Q^2 \approx 0$.

342 The final state bremsstrahlung electrons provide a powerful tool for calibrating and ver-
 343 ifying the luminosity measurement with photons. Tagging bremsstrahlung electrons and
 344 counting corresponding photons in the photon detectors provides a direct measure of the
 345 luminosity detector acceptance in the tagged energy range. This is of paramount impor-
 346 tance to precisely determine the pair conversion probability for the luminosity spectrome-
 347 ter, which depends on the exit window composition and thickness.

348 Tagging of low- Q^2 processes provides an extension of the kinematic range of DIS pro-
 349 cesses measured with electrons in the central detector. It crosses the transition from DIS to
 350 hadronic reactions with quasi-real photons. An example of acceptance as a function of Q^2
 351 for measurements with the central detector and electron taggers as depicted in Fig. ?? is
 352 shown in Fig. 6. The electrons are generated by a simple model of quasi-real photoproduc-
 353 tion [19] and Pythia. The taggers provide useful acceptance in the range $10^{-6} < Q^2 < 10^{-2}$
 354 GeV^2 . Application of the electron taggers for low- Q^2 physics will face a challenge from the
 355 high rate bremsstrahlung electrons, which can be addressed by tagger design and correla-
 356 tion with information from the central detector.

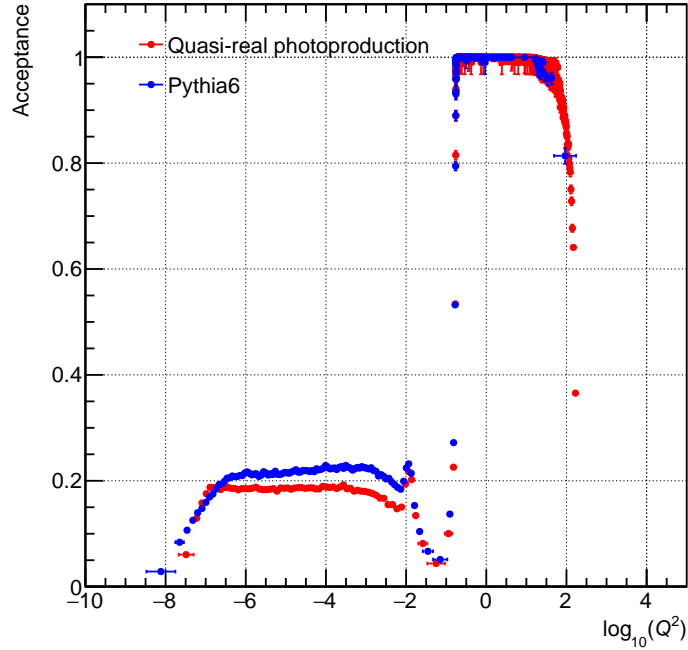


Figure 6: Acceptance as a function of Q^2 for electrons measured in the central detector (right plateau) and downstream taggers (left plateau). The electrons are generated by a simple model of quasi-real photoproduction and Pythia.

357 Possible locations of detectors for these electrons are shown in the top left of Fig. ?. Elec-

358 trons with energies slightly below the beam are bent out of the beam by the first lattice
359 dipole after the interaction point. The beam vacuum chamber must include exit windows
360 for these electrons. The windows should be as thin as possible along the electron direction
361 to minimize energy loss and multiple scattering before the detectors.

362 The taggers should include calorimeters for triggering and energy measurements. They
363 should be finely segmented to disentangle the multiple electron hits per bunch crossing
364 from the high rate bremsstrahlung process. The taggers should also have position sensi-
365 tive detectors to measure the vertical and horizontal coordinates of electrons. The com-
366 bined energy and position measurements allow reconstruction of the kinematic variable
367 Q^2 and x_{BJ} . If the position detectors have multiple layers and are able to reconstruct the
368 electron direction this will overconstrain the variable reconstruction and improve their
369 measurement; this may also provide some measure of background rejection. The beam
370 angular divergence will introduce significant errors on the variable reconstruction. The re-
371 constructed versus generated Q^2 is shown in Fig. 7 with smearing from beam divergence.
372 There is reasonable resolution for Q^2 as low as 10^{-3} GeV²; below 10^{-4} GeV² meaningful
373 reconstruction of Q^2 based on the electron is not possible.

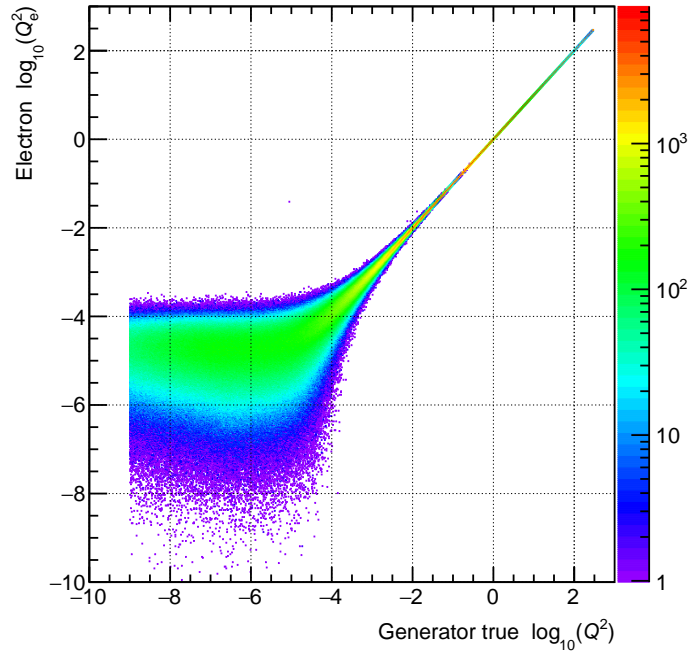


Figure 7: Comparison of reconstructed and reconstructed electron Q_e^2 with smearing for beam angular divergence.

References

374

- 375 [1] K. Aulenbacher, E. Chudakov, D. Gaskell, J. Grames, and K. D. Paschke, "Precision
376 electron beam polarimetry for next generation nuclear physics experiments," *Int. J.*
377 *Mod. Phys. E*, vol. 27, no. 07, p. 1830004, 2018.
- 378 [2] J. Hansknecht and M. Poelker, "Synchronous photoinjection using a frequency-
379 doubled gain-switched fiber-coupled seed laser and ErYb-doped fiber amplifier,"
380 *Phys. Rev. ST Accel. Beams*, vol. 9, p. 063501, 2006.
- 381 [3] B. Sobloher, R. Fabbri, T. Behnke, J. Olsson, D. Pitzl, S. Schmitt, and J. Tomaszewska,
382 "Polarisation at HERA - Reanalysis of the HERA II Polarimeter Data -," *HERA Internal*
383 *Note*, 1 2012.
- 384 [4] A. Camsonne, J. Hoskins, *et al.*, "eRD15: R&D for a Compton Electron Detector," *EIC*
385 *R&D Progress Report*, June 2017.
- 386 [5] A. Camsonne, J. Hoskins, *et al.*, "eRD15: R&D for a Compton Electron Detector," *EIC*
387 *R&D Progress Report*, January 2016.
- 388 [6] F. Méot *et al.*, "eRHIC EIC: Plans for Rapid Acceleration of Polarized Electron
389 Bunch at Cornell Synchrotron," in *9th International Particle Accelerator Conference*,
390 p. MOPMF013, 2018.
- 391 [7] W. B. Schmidke *et al.*, "Rhic polarization for runs 9-17," Tech. Rep. BNL-209057-2018-
392 TECH, C-A/AP/609, Brookhaven National Laboratory, 2018. [https://technotes.](https://technotes.bnl.gov/PDF?publicationId=209057)
393 [bnl.gov/PDF?publicationId=209057](https://technotes.bnl.gov/PDF?publicationId=209057).
- 394 [8] A. A. Poblaguev, A. Zelenski, G. Atoian, Y. Makdisi, and J. Ritter, "Systematic error
395 analysis in the absolute hydrogen gas jet polarimeter at RHIC," *Nucl. Instrum. Meth.*
396 *A*, vol. 976, p. 164261, 2020.
- 397 [9] A. Zelenski *et al.*, "Absolute polarized H-jet polarimeter development, for RHIC,"
398 *Nucl. Instrum. Meth. A*, vol. 536, pp. 248–254, 2005.
- 399 [10] W. Fischer and A. Bazilevsky *Phys. Rev. ST Accel. Beams*, vol. 15, p. 041001, 2012.
- 400 [11] C. Aidala *et al. Phys. Rev. Lett.*, vol. 120, p. 022001, 2018.
- 401 [12] G. Mitsuka *Phys. Rev.*, vol. C95, p. 044908, 2017.

- 402 [13] N. H. Buttimore, B. Kopeliovich, E. Leader, J. Soffer, and T. Trueman, "The spin de-
403 pendence of high-energy proton scattering," *Phys. Rev. D*, vol. 59, p. 114010, 1999.
- 404 [14] A. A. Poblaguev *et al.*, "Precision Small Scattering Angle Measurements of Elastic
405 Proton-Proton Single and Double Spin Analyzing Powers at the RHIC Hydrogen Jet
406 Polarimeter," *Phys. Rev. Lett.*, vol. 123, no. 16, p. 162001, 2019.
- 407 [15] G. Atoian, A. Zelenski, and A. Poblaguev, "Precision absolute polarimeter develop-
408 ment for the 3He⁺⁺ ion beam at 5.0–6.0 MeV energy," *PoS*, vol. PSTP2019, p. 045,
409 2020.
- 410 [16] H1 Luminosity Monitor, <http://www-h1.desy.de/h1/www/h1det/lumi/>.
- 411 [17] F. D. Aaron *et al.*, "Determination of the Integrated Luminosity at HERA using Elastic
412 QED Compton Events," *Eur. Phys. J.*, vol. C72, p. 2163, 2012. [Erratum: *Eur. Phys.*
413 *J.*C74,2733(2012)].
- 414 [18] Zeus Luminosity Monitor, [http://www-zeus.desy.de/zeus_](http://www-zeus.desy.de/zeus_det_papers/zeus_)
415 [det_papers.html](http://www-zeus.desy.de/zeus_det_papers/zeus_det_papers.html).
- 416 [19] U. Amaldi, ed., *Study of an ep Facility for Europe DESY, Hamburg, April 2-3, 1979.*,
417 vol. 790402, (Hamburg, Germany), Deutsches Electron Synchrotron / European Com-
418 mittee for Future Accelerators, 1979.